Available online at www.sciencedirect.com
SCIENCE DIRECT®
Estuarine, Coastal and Shelf Science 57 (2003) 1183–1193
ESTUARINE COASTAL AND SHELF SCIENCE

Pyritization: a palaeoenvironmental and redox proxy reevaluated

Alakendra N. Roychoudhury[a,*], Joel E. Kostka[b], Philippe Van Cappellen[c]

[a]Department of Geological Sciences, University of Cape Town, Rondebosch 7700, South Africa
[b]Department of Oceanography, Florida State University, Tallahassee, FL 32306, USA
[c]Department of Geochemistry, Utrecht University, P.O. Box 80021, 3508 Utrecht, The Netherlands

Received 12 November 2002; accepted 29 January 2003

Abstract

Pyrite as a proxy for the redox states of bottom waters was evaluated in the context of modern salt marsh sediments. Two sites, 40 m apart, with very different physicochemical properties were sampled seasonally. The sites differed from each other in (1) the amount of tidal flushing, (2) vegetation, (3) redox condition below the sediment–water interface, (4) carbon content and (5) solid phase iron oxyhydroxide and iron sulfide content of the sediment. The calculated degree of pyritization (DOP) varies between 0.44 and 1.0, depending on the site and the season. Different DOP values were obtained for the same samples when different techniques were applied for extraction of reactive iron. Framboidal pyrite was dominant; however, other textural forms of pyrite were also observed. The size distribution of the individual pyrite crystals and the framboids was fairly narrow; with the majority of them having diameters <10 μm. Despite deposition taking place in aerobic waters (fully oxygenated waters) at the sampled sites, both the DOP and pyrite textures indicated dysoxic (waters with low oxygen concentrations) to euxinic (waters with no oxygen present, and H_2S may be continually or intermittently present) bottom waters. These results indicate that caution must be applied when using DOP and pyrite morphologies as proxies for interpreting the redox conditions of different depositional environments.

Keywords: degree of pyritization; iron; proxy; pyrite; redox; saltmarsh; sulfur

1. Introduction

Biogeochemical proxies are widely used for reconstructing geological events and identifying periodically changing environmental conditions (Henderson, 2002). Redox state(s) has always been a key environmental factor to be investigated as it exerts a major control over coupled biogeochemical cycles and is also linked to the evolution and diversification of life on earth (Berner, 1989; Berner & Landis, 1988; Buick, 1992; Grandstaff, 1980; Runnegar, 1991; Schidlowski, Appel, Eichmann, & Junge, 1979; Schidlowski, Junge, & Pietrek, 1977).

Formation and accumulation of pyrite during early diagenesis is controlled by a number of environmental determinants including availability of iron, sulfate, organic carbon, pyrite oxidation rate and hydrodynamics (Berner, 1970, 1982, 1984; Luther, Giblin, Howarth, & Ryans, 1982; Morse & Wang, 1997; Raiswell & Berner, 1985; Raiswell & Canfield, 1998). The notion of stability of pyrite, and the fact that most marine sediments and sedimentary rocks contain at least traces of pyrite (Berner, 1982), has resulted in the formation of pyrite being widely used as a proxy to identify a variety of redox controlled cyclic transitions and depositional environments (Boesen & Postma, 1988; Raiswell & Berner, 1985; Raiswell, Buckley, Berner, & Anderson, 1988; Raiswell, Canfield, & Berner, 1994; Suits & Wilkin, 1998; Wilkin, Arthur, & Dean, 1997). Pyrite surface morphologies and degree of pyritization (DOP) are often applied for the identification of the palaeo-redox status.

DOP is operationally defined as (Berner, 1970),

$$\mathrm{DOP} = \frac{\%\mathrm{Fe}_{\mathrm{pyrite}}}{\%\mathrm{Fe}_{\mathrm{pyrite}} + \mathrm{Reactive\ Fe}} \quad (1)$$

$\mathrm{Fe}_{\mathrm{Pyrite}}$ is the fraction of iron associated with pyrite. The reactive Fe is defined as the fraction of iron that

* Corresponding author.
E-mail address: aroy@geology.uct.ac.za (A.N. Roychoudhury).

0272-7714/03/$ - see front matter © 2003 Elsevier Ltd. All rights reserved.
doi:10.1016/S0272-7714(03)00058-1

readily reacts with dissolved sulfide to produce iron monosulfides and eventually pyrite. Berner (1970) extracted the reactive Fe by boiling the sediments in concentrated HCl for 1 min.

Based on a comprehensive analysis of ancient shale formations, Raiswell et al. (1988) have proposed that sediments with DOP of <0.46 indicate aerobic bottom water conditions; dysoxic or restricted conditions are implied by a DOP value between 0.46 and 0.75 and a DOP of >0.75 suggests euxinic conditions for the deposition of fine grained sediments (Raiswell et al., 1988). Others have used DOP to demonstrate iron or sulfur limitation in pyrite formation, for example, DOP values close to unity suggest iron limitation (Berner, 1970; Dean & Arthur, 1989; Raiswell & Berner, 1985).

During early diagenesis, the majority of pyrite precipitates as spherical framboids formed by aggregation of submicron size individual particles, or as single or clustered euhedral crystals (Wilkin, Barnes, & Brantley, 1996). In euxinic bottom waters, framboidal pyrite is formed at the oxic–anoxic transition by replacement of more sulfide rich phases (Wilkin et al., 1996). The initial reaction rate is fast, which allows formation of pyrite within the water column, and the framboidal spheres are generally <10 μm in diameter (Wilkin & Barnes, 1997a; Wilkin et al., 1996). Euhedral crystals result when the initial rate of pyritization is slow (Morse & Wang, 1997; Wilkin & Barnes, 1996); therefore, they usually form within the sediments where sulfide has more time to react with the precursor minerals to form pyrite. Diagenetic framboids are also common; however, secondary growth and in-filling is often associated with them. Because of these differences, Wilkin and others have proposed the use of size and texture of pyrite to differentiate syngenetic and diagenetic pyrite and thereby account for bottom water oxygen conditions (Suits & Wilkin, 1998; Wignall & Newton, 1998; Wilkin & Arthur, 2001; Wilkin et al., 1997, 1996; Wilkin & Barnes, 1996, 1997a,b).

Although, pyrite morphologies and DOP has been successfully applied to establish palaeo-depositional redox conditions in subtidal marine environments, these criteria may not be universally applicable to other depositional environments, such as those of the intertidal zone. In this article, the implications of using these palaeoenvironmental indicators for sediments depositing within the dynamic setting of an estuary are discussed.

2. Materials and methods

2.1. Site description and sediment

Sediment samples were collected from a salt marsh mud flat at the southern end of Sapelo Island (Georgia, USA). A medium size tidal creek flows through the southwest end of the marsh, and *Spartina alterniflora* constitutes the dominant vegetation. A sedimentation rate of 1–3 mm $year^{-1}$ has been estimated previously at Sapelo Island (Howarth & Giblin, 1983). The sediments were collected in May (1997) and January (1998) from the unvegetated tidal creek bank (Creek Bank) and from the vegetated portion of the marsh (Ponded Marsh), 40 m away from the creek bank (Fig. 1). The sites differed from each other in the amount of tidal flushing, redox condition below the sediment–water interface, carbon content and solid phase iron oxyhydroxide and iron sulfide content of the sediment. Twice every day, the sites are inundated by tidal water for 3–4 h. Strong tidal flushing is observed at the Creek Bank site; however, the water movement is restricted at Ponded Marsh. Oxygen concentration in the tidal water varies between 100 and 170 μM seasonally (Cai et al., personal communication). Fiddler crab burrows, sometimes reaching a depth of 40–45 cm, are found at both sites, with a higher abundance observed at the Creek Bank site (Kostka, Roychoudhury, & Van Cappellen, 2002). These observations are in relative agreement with the previous estimates of crab burrow aperture densities of 1040 and 414 per m^2 at the Creek Bank and Ponded Marsh sites, respectively (Basan & Frey, 1977). In addition, the macroinvertibrates at the two sites continuously rework the top 3–8 cm of sediment through bottom feeding activities (Kostka et al., 2002). Due to bioirrigation, enhanced oxygen flux of 8.1 ± 1.1–117 ± 115 mmol O_2 m^{-2} d^{-1} to the sediments has been estimated (Meile, Koretsky, & Van Cappelen, 2001); however, most of the oxygen is consumed within a depth of 2–4 mm below the sediment–water interface (Cai et al., personal communication). *Spartina* roots at the Ponded Marsh site provide an additional conduit for the diffusion of oxygen below the surface, creating oxic microcosms around the roots that are predominantly surrounded by anaerobic sediments (Dacey & Howes, 1984; Howes, Dacey, & Goehringer, 1986; Luther et al., 1982).

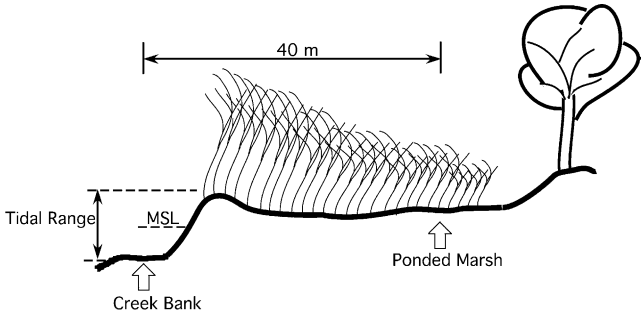

Fig. 1. Schematic figure of the sampling area. Note that during high tides, water flows over the levee and the Ponded Marsh site is submerged under water. At low tides, the Creek Bank site is exposed to the atmosphere.

2.2. Sediment and pore water collection and characterization

Sediments were collected using a wedge corer that minimizes compaction (Inglette et al., in review). Once a core was retrieved, it was transferred to the field laboratory within 30 min and sectioned at desired depth intervals inside a glove bag in less than 2 h. Sediment sections were double bagged under nitrogen and frozen for transportation to the laboratory where a portion of each sediment section was freeze-dried within a week. Size analysis of the coarser sediments was done by sieving (ASTM, D 422-63, Reapproved, 1990). Finer sediments were suspended in deionized water, sonicated and analyzed by a laser-based particle size analysis system (Brinkman, Model 2010). Porosity was determined by measuring the weight loss of a saturated sediment section packed in a 1-ml syringe after air-drying it. Density was calculated by measuring the weight of sediment in the same syringe used for porosity determination.

Total carbon in the sediment samples was measured by high temperature (900–1000 °C) combustion, followed by CO_2 titration (Coulometrics, Model 5022). The inorganic (carbonate) carbon content of the sediments was obtained by titrating CO_2 released after treating the samples with a 2 N H_2SO_4 solution. The organic carbon concentration was calculated as the difference between total and inorganic carbon.

Solid phase sulfides (acid volatile sulfides ($H_2S + FeS$) and chromium reducible sulfides ($FeS_2 + S^0$) referred to henceforth as AVS and CRS), respectively, were measured on frozen sediment samples by a two step distillation process modified after Canfield, Raiswell, Westrich, Reaves, and Berner (1986) and Fossing and Jørgensen (1989). In comparison with pyrite, S^0 concentrations in salt marsh sediment are expected to be negligible (Cutter & Velinsky, 1988). Therefore, for all practical purposes, CRS represents pyritic sulfur in this study. All concentrations are reported on a dry sediment weight basis.

Different definitions for reactive iron exist in the literature (Berner, 1970, 1982; Canfield, 1989; Kostka & Luther, 1994), and as such, different techniques for its extraction have also been applied in the past. Reactive Fe was quantified using three different extraction procedures to identify their effect on DOP calculations: (1) 1 M cold HCl extraction (Leventhal & Taylor, 1990), (2) ascorbate extraction (Kostka & Luther, 1995) and (3) a sequential extraction method modified after Canfield (1989) and Kostka and Luther (1995). For the sequential extraction, the following leachates and extraction times were used:

1. Ascorbate solution (pH 8): 4 g ascorbic acid + 10 g sodium citrate + 10 g sodium bicarbonate in 200 ml deionized water—24 h
2. 1 N cold HCl—1 h
3. 0.2 M ammonium oxalate—2 h
4. Buffered sodium dithionite (pH 2): 0.5 g sodium dithionite per 10 ml of buffer solution (0.2 M sodium citrate + 0.35 M acetic acid buffer)—3 h

Total reactive iron was calculated by adding the individual iron fractions extracted sequentially. Note that the total reactive iron is equal to the iron extracted if the sediments are treated with buffered sodium dithionite as the sole leachate (Canfield, 1989; Roychoudhury, 1999) but is not equivalent to the total iron that is extracted by whole sediment digestions using a $HF–HNO_3$ mixture. All extractable iron concentrations are also reported on a dry sediment weight basis.

DOP was calculated using the following equation:

$$\mathrm{DOP} = \frac{0.5 \times [\mathrm{CRS}]}{0.5 \times [\mathrm{CRS}] + \text{Reactive Fe}}, \quad (2)$$

where [CRS] denotes the concentration of CRS.

Pyrite grain morphology was observed under a scanning electron microscope (SEM) (Leo S440) coupled to a Centaurus back-scatter detector and a Microanalysis Link-Kevex (EDX) detector, which had been calibrated with a 99.99 Cu stub with or without Be window. Samples were prepared by sprinkling dry sediment over a stub pretreated with a mixture of carbon and glue and coating them with a thin film of carbon using the evaporation technique. Sulfate reduction rates (SRR) were determined with $^{35}SO_4^{2-}$ labeled short-term sediment incubations at in situ temperatures (Jørgensen, 1978). Reduced ^{35}S was recovered using a two step distillation process in order to calculate the reduction rates (Canfield et al., 1986; Fossing & Jørgensen, 1989). Pore waters were collected using peepers (Hesslein, 1976). The peepers were inserted into the sediments and left to equilibrate with the pore waters. After 1 month, they were recovered and at once placed inside a glove bag. Pore waters were retrieved directly in syringes and filtered using a 0.45 μm nylon flow-through filter. Filtered samples were distributed in different aliquots for analysis and preservation. Sulfide was analyzed immediately after filtration (Cline, 1969) and one aliquot was preserved in 0.5 M HCl for analyzing sulfate by the turbidimetric method (Tabatabai, 1974).

3. Results

3.1. Sediments

Creek Bank sediments are heterogeneous, with an intermix of sand, silt and clay size particles (average grain size diameter = 200 μm; porosity = 0.76 ± 0.02; density = 1.34 ± 0.04 g cm^{-3}). The sediments are brownish to grayish in color up to 25–30 cm below the

sediment–water interface, indicating a large suboxic zone. A more blackish color was observed below those depths. Except for a few intermittent peaks, carbon content was constant with depth in May ($3.71 \pm 0.85\%$; $\pm 2\sigma$, $n = 10$). But in January, carbon content decreased from 4.4 to 2.3% by a depth of 43 cm from the sediment–water interface. Inorganic carbon content was low (0.20%).

At the Ponded Marsh site, sediments are black in color and homogeneous with mostly clay size particles (average grain size diameter = 0.2 μm; porosity = 0.82 ± 0.04; density = 1.26 ± 0.09 g cm^{-3}). Occasional sand lenses occur within the sediment. An extensive root zone extends to depths of 15–20 cm. Even though the site was vegetated with *Spartina* grass, the organic carbon content of the sediment was not very high (4.85%) compared with values reported in the literature (11–43%) from other east coast salt marshes (Barnes, Craft, & Windom, 1973). A negligible amount of inorganic carbon (0.15%) was found in the sediment. For both seasons, carbon content gradually decreased down core by approximately 30% with depth.

3.2. Solid phase iron

At Creek Bank, neither depth integrated (0–35 cm) total extractable reactive iron (May—6.22 mmol cm^{-2}, January—6.21 mmol cm^{-2}) nor ascorbate extractable iron (May—3.08 mmol cm^{-2}, January—3.04 mmol cm^{-2}) change significantly between seasons. During sequential extractions, only the ascorbate extractable iron profile showed a distinct gradient with depth (Fig. 2.1a, 2.2a). A high concentration (100–160 μmol cm^{-3}) of ascorbate extractable iron was present up to a depth of 10–15 cm, below which it decreased almost exponentially to 40–60 μmol cm^{-3} by a depth of 30–40 cm (Fig. 2.1a, 2.2a). HCl extractable iron concentrations extracted using the method of Leventhal and Taylor (1990) were much higher than those obtained during sequential extraction or using the ascorbate extraction (Table 1).

At Ponded Marsh, ascorbate extractable iron content in the month of May was relatively low (~80 μmol cm^{-3}) at the surface. A rapid decrease to about 10 μmol cm^{-3} was observed within the first 6 cm, below which values remain constant (Fig. 2.3a). In January, concentrations were lower in the surface sediments and except for one anomalous peak at 36 cm the concentrations were nearly constant with depth (Fig. 2.4a). However, depth integrated (0–35 cm) ascorbate extractable reactive iron content was higher by a factor of four in January (2.03 mmol cm^{-2}) compared with that in May (0.50 mmol cm^{-2}). Change in total extractable reactive iron between seasons was not as significant (May—3.22 mmol cm^{-2}, January—4.28 mmol cm^{-2}). At Ponded Marsh also, highest iron concentrations were extracted by the method of Leventhal and Taylor (1990) (Table 1).

3.3. Solid phase sulfides

At Creek Bank, depth integrated (0–35 cm) AVS was low (0.47–1.03 mmol(S) cm^{-2}). An increasing trend in the AVS concentrations with depth was observed in May (Fig. 2.1a). Surprisingly, AVS accumulated more in January when SRR were lower (Table 1, Fig. 2.2b, 2.2c) and pore waters were comparatively more oxygenated than in May (see DOP values, Table 1). A peak was observed around 22 cm, below which AVS decreased almost exponentially (Fig. 2.2b). Even though depth integrated SRR were highest at Creek Bank, CRS concentrations were substantially lower than those observed at Ponded Marsh. However, most of the sulfur was tied as CRS (17.80–29.95 mmol (S) cm^{-2}) and pyrite concentrations did not fluctuate significantly with depth (Fig. 2.1b, 2.2b).

At Ponded Marsh in May, the highest concentration of AVS (~120 μmol cm^{-3}) was observed in the top 1 cm, below which concentrations decrease exponentially (Fig. 2.3b). The peak concentration shifted downwards in January and again an exponential decrease was observed below the maxima (Fig. 2.4b). Depth integrated (0–35 cm) AVS did not change substantially between seasons (May—0.89 mmol(S) cm^{-2}, January—0.93mmol(S) cm^{-2}). At Ponded Marsh also, most of the sulfur was tied in the CRS form and concentrations increased gradually with depth (Fig. 2.3b, 2.4b). Intermittent peaks are observed between 5 and 8 cm below the sediment–water interface (Fig. 2.3b) and are mostly associated with the *Spartina* roots. The depth integrated (0–35 cm) CRS concentration was higher by a factor of four in May (190.91 mmol(S) cm^{-2}) compared with that in January (47.20 mmol(S) cm^{-2}).

3.4. Degree of pyritization

Based on how reactive Fe is extracted, calculated DOP values vary at both sites (Table 1). Ascorbate extractable reactive iron provided the highest value of DOP, whereas the lowest DOP values are obtained when HCl extractable reactive iron is used in Eq. (2). Also, irrespective of the extraction procedure used, Ponded Marsh samples consistently had higher DOP compared with Creek Bank sediments (Table 1).

3.5. Pyrite grain morphologies

At Sapelo Island salt marsh, pyrite occurs as individual or clustered framboids and octahedral crystals, as anhedral grains and possibly as unidentifiable fine dispersed grains (Fig. 3). All of the pyrite grains analyzed were <12 μm in size, with the majority of them below 5 μm. Framboidal texture dominated in most of the samples analyzed.

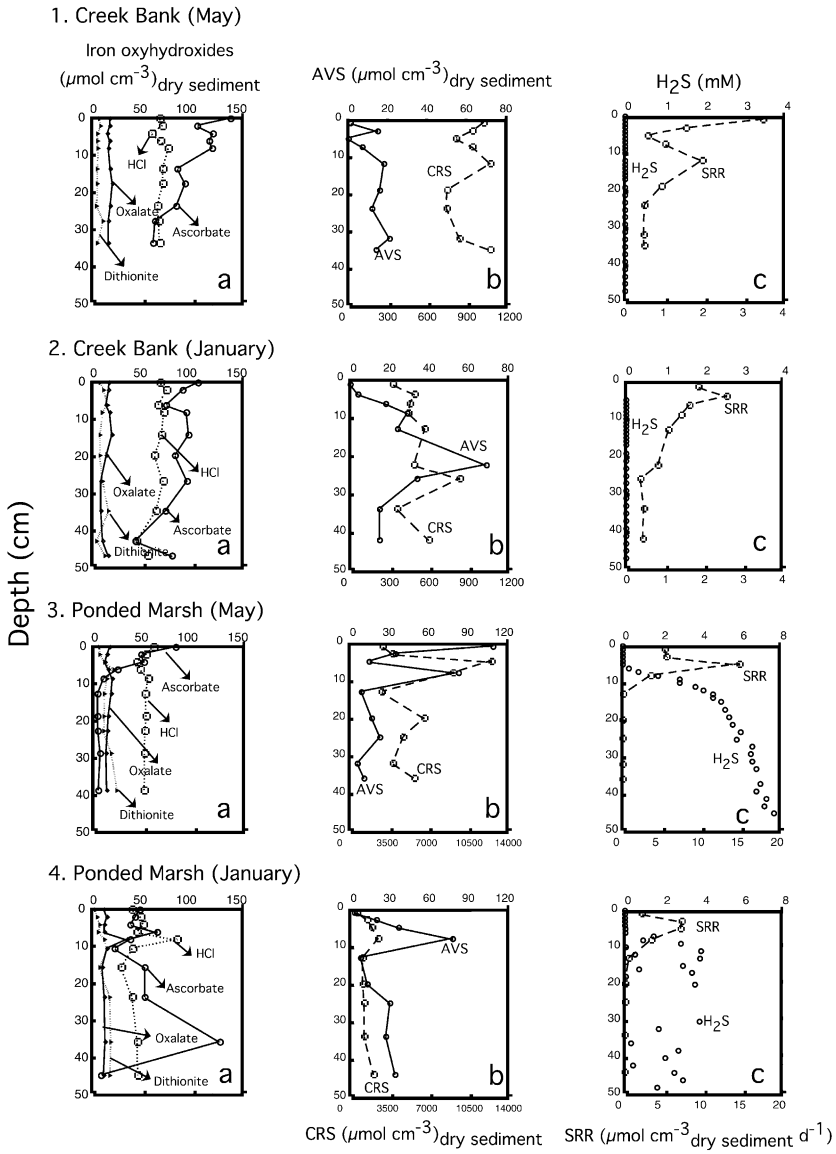

Fig. 2. Depth distribution profiles of (a) sequentially extracted solid phase iron, (b) solid phase AVS and CRS and (c) dissolved sulfide and SRR. The data plotted are the average of duplicate measurements.

At Creek Bank site, although pyrite concentrations were $>300\,\mu mol\,cm^{-3}$ throughout the sampled depths at all times, pyrite grains were hard to locate, especially at depths <5 cm below the sediment–water interface. It seems that the majority of the pyrite at those depths occurs in the form of fine anhedral grains, which are hard to identify, although a few nanometer scale clusters of two or three fused euhedral crystals were observed (Fig. 3a). Framboids were more frequent at greater depths and in-filled pyrite framboids were mostly found at depths >20 cm (Fig. 3b).

At Ponded Marsh, pyrite grains were easier to spot under a SEM at all depths. Single or clustered euhedral crystals were observed at shallower depths or in samples from the root zone where concentrated pockets of disaggregated individual euhedral crystals and framboids were found (Fig. 3d,f,g). In one sample, euhedral crystals were observed as deep as 42 cm below the sediment–water interface. Framboid morphology dominated at all depths, although perfectly spherical framboids were not observed. Comparatively large diameter framboids (6–1 μm) were observed at depths <10 cm (Fig. 3e). At greater depths, framboids of diameter >7 μm were ubiquitously absent and fused framboids were far more frequent (Fig. 3h).

4. Discussion

4.1. Degree of pyritization

At two sampling sites, 40 m apart from each other within the same salt marsh mud flat, markedly different

Table 1
Calculated DOP and solid phase concentrations of reactive iron and sulfides at the two sites (note that different DOP values are based on the reactive iron dissolved by various extraction methods used in this study)

	Sulfide (μmol cm^{-3})$_{\text{Dry sediment}}$		Reactive iron (μmol cm^{-3})$_{\text{Dry sediment}}$			DOP		
Depth (cm)	AVS	CRS	Ascorbate extractable	Dithionite[a] extractable	HCl extractable	Ascorbate iron	Dithionite iron	HCl iron
Creek Bank (May)								
0.5	0.7	1028	138	230	220	0.79	0.69	0.70
2.5	14.9	942	105	201	264	0.82	0.70	0.64
4.5	0.3	818	120	201	268	0.77	0.67	0.60
6.5	6.9	944	117	208	248	0.80	0.69	0.66
14	17.8	1081	85	179	230	0.86	0.75	0.70
18	16.0	753	93	188	255	0.80	0.67	0.60
24	12.0	748	84	171	235	0.82	0.69	0.61
28	20.7	846	63	156	168	0.87	0.73	0.72
35	14.3	1079	61	150	207	0.90	0.78	0.72
Creek Bank (January)								
0.5	0.4	325	105	197	205	0.61	0.45	0.44
2.5	4.0	490	90	191	230	0.73	0.56	0.52
6.5	17.5	454	74	168	194	0.75	0.57	0.54
8.5	28.7	444	94	192	230	0.70	0.54	0.49
14.5	23.6	568	96	192	271	0.75	0.60	0.51
20	69.0	486	82	166	283	0.75	0.59	0.46
27	34.3	833	95	184	309	0.82	0.69	0.57
35	14.6	358	73	161	251	0.71	0.53	0.42
43	14.9	600	43	102	220	0.87	0.75	0.58
Ponded Marsh (May)								
0.5	109.1	2941	82	165	250	0.95	0.90	0.85
2.5	35.0	3791	48	120	403	0.98	0.94	0.82
4.5	15.0	12,583	51	117	162	0.99	0.98	0.97
6.5	82.6	9177	24	106	155	0.99	0.98	0.97
13	9.0	2832	4	84	115	1.00	0.94	0.93
19	17.2	6606	4	82	147	1.00	0.98	0.96
23	23.1	4745	5	80	138	1.00	0.97	0.95
29	6.1	3843	6	88	125	1.00	0.96	0.94
39	11.2	5741	5	92	109	1.00	0.97	0.96
Ponded Marsh (January)								
0.5	2.8	603	48	103	186	0.86	0.75	0.62
2.5	20.2	1516	43	111	291	0.95	0.87	0.72
4.5	36.6	1942	38	109	213	0.96	0.90	0.82
6.5	78.1	2475	65	128	199	0.95	0.91	0.86
11	7.5	1104	22	92	69	0.96	0.86	0.89
16	13.2	1106	52	99	113	0.91	0.85	0.83
24	30.3	1223	52	122	110	0.92	0.83	0.85
36	27.2	1263	128	204	68	0.83	0.76	0.90
45	34.4	2060	9	83	105	0.99	0.93	0.91

[a] Dithionite extractable iron was calculated from the sequential extraction by summing individual fractions of iron extracted at each step (for details see Section 2).

DOP was observed. Although oxygen measurements (Cai et al., unpublished results) demonstrate that deposition is taking place under an aerobic water column, the DOP values suggest dysoxic bottom water conditions for the Creek Bank site and euxinic conditions for the Ponded Marsh site. Further confusion and variation in DOP values result when different extraction techniques are used for quantifying reactive iron.

One of the issues related to the extraction techniques is which method best quantifies the reactive iron phase that is available for pyrite formation. Berner (1970) quantified the 'most reactive iron (towards H_2S)' using 12 N hot HCl. Later, Leventhal and Taylor (1990) showed that in natural sediments 1 N cold HCl extraction is more convenient and provides similar results as the hot extraction. However, based on calibrations with pure mineral phases, the cold extraction technique was criticized by Raiswell et al. (1994) for not extracting lepidocrocite, goethite and hematite, phases that are readily converted to iron sulfides in modern sediments. Raiswell et al. (1994) further proposed the use of dithionite extraction for modern sediments. In this study, 1 N cold HCl extraction provided similar results to dithionite extraction, probably because in salt marsh

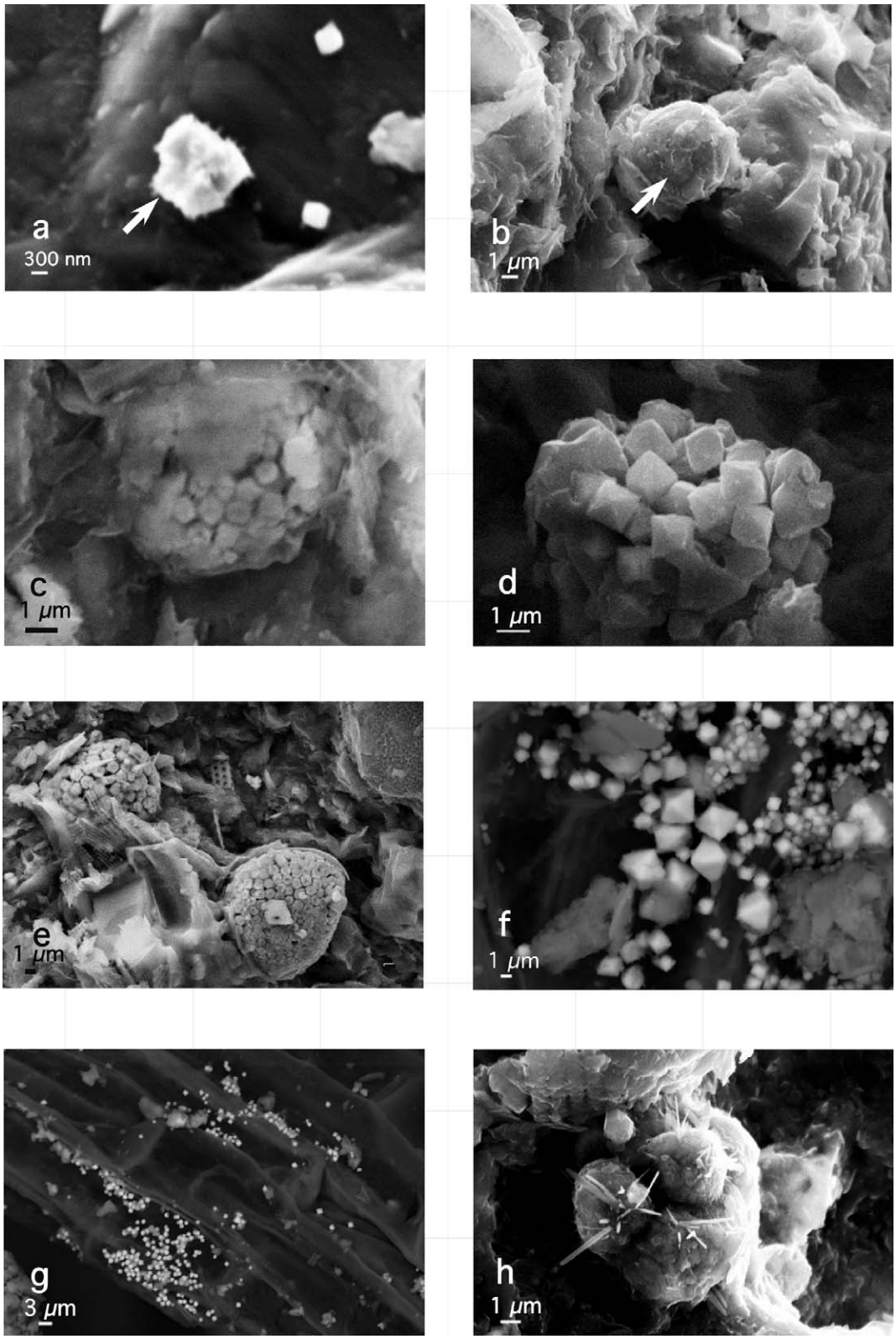

Fig. 3. Scanning electron micrographs showing various pyrite textures and grain sizes observed at the Sapelo Island saltmarsh sediments: (a) arrow-head shows poorly developed and fused octahedral pyrite crystals at the Creek Bank site, (b) arrow-head points to the fused framboid observed at the Creek Bank site, (c) in-filled framboid at Ponded Marsh site, (d) cluster of well developed octahedral crystals, (e) framboidal pyrite made up of uniform microcrystals, (f) loose as well as clustered pyrite crystals concentrated around *Spartina* root, (g) concentrated pockets of pyrite crystals around *Spartina* root and (h) cluster of fused framboids formed around a diatom.

sediments reductive dissolution of hematite and magnetite is catalyzed by Fe(II)–organic acid complexes (Kostka & Luther, 1994). However, this does not necessarily mean that dithionite extraction or HCl extractions dissolve iron phases that are reacting to form pyrite.

On a time scale of hundreds to thousands of years, provided organic carbon and sulfate are not limiting, iron associated with all the phases (oxides, silicates, amphiboles and others) is potentially available for pyrite formation (Canfield, Raiswell, & Bottrell, 1992). However, during early diagenesis only the most reactive part of iron is pyritized. From sequential extractions, it becomes apparent that only the ascorbate extractable phase is depleted with depth, suggesting that this phase is reacting to form pyrite (see Fig. 2.1a, 2.2a, 2.3a). Both dithionite and HCl extractions overestimate the iron that undergoes pyritization, especially at greater depths (Table 1). It is possible that both dithionite and HCl are extracting phases associated with relatively less reactive silicates that do not undergo pyritization easily.

Irrespective of the extraction procedure used, the calculated DOP values are higher than expected for sediments deposited in an aerobic environment (Table 2). The DOP values obtained here are comparable with dysoxic to euxinic depositional environments (Table 2). In fact, for the two sites, the calculated DOP values predict dysoxic conditions at the Creek Bank site and euxinic conditions for the Ponded Marsh site (see Tables 1 and 2). Furthermore, the relatively constant value of DOP with depth at Creek Bank can further be interpreted as pyritization being complete at or above the sediment–water interface (see Lyons & Berner, 1992; Wilkin et al., 1997). Such obviously erroneous interpretations suggest that DOP may not always differentiate between syngenetic and diagenetic pyrite or predict correctly the bottom water oxygen conditions during sediment deposition. What's more, DOP values from ancient sediment deposits show an overlap between dysoxic ($0.46 < \mathrm{DOP} < 0.87$) and euxinic ($0.55 < \mathrm{DOP} < 1.00$) environments (Table 2) (Raiswell et al., 1988). It is possible that the high DOP values in dysoxic environments were caused by depositional conditions similar to those observed in the modern salt marsh system.

A note must be made here regarding the use of CRS concentrations in Eq. (2) to denote pyritic iron. Since CRS extracts S^0 along with FeS_2, some overestimation of pyritic iron would result when measured sulfur concentrations are converted to Fe equivalents using a 2 : 1 S to Fe ratio. However, this overestimation only means that the calculated DOP values are representing more oxygenated conditions, that is, the environment, in fact, should be more reducing. However, this interpretation is further away from the demonstrated fact that the bottom waters are aerobic.

The DOP values at the two sites are largely controlled by the rate of sulfate reduction and tidal flushing, and to a lesser extent by bioturbation and macrophytes. At the Creek Bank site, depth integrated SRR were the highest observed, although no accumulation of dissolved sulfide occurs. (Fig. 2.1c, 2.2c). This is due to the site's proximity to the tidal channel. Twice daily, the influx of tidal water laterally transports oxygen to all depths that oxidize excess sulfide and replenishes iron oxyhydroxides. The combination of high SRR and regular infusion of oxygen result in dysoxic conditions below the sediment–water interface. At Ponded Marsh, water movement is restricted. Even though the site is inundated by tidal water diurnally, a high water table at the site and impermeable clays do not allow oxygenated water to percolate below the surface. Combined with this, high SRR close to the sediment–water interface (Fig. 2.3c, 2.4c) results in complete oxygen consumption within the first few millimeters below ground. This allows the build up and downward diffusion of sulfide in the pore waters, resulting in euxinic conditions. Thus, it appears that at both sites the DOP values are reflective of the sediment chemistry and pore water redox conditions rather than the bottom water conditions under which sediment deposition and pyritization is taking place.

Table 2
A comparison of DOP calculated during this study with those obtained from other ancient depositional environments

Site	Degree of bottom water oxygenation	DOP
Modern saltmarsh sediments Sapelo Island, USA (Creek Bank)	Aerobic	0.44–0.72[a]
Modern saltmarsh sediments Sapelo Island, USA (Ponded Marsh)	Aerobic	0.62–0.97[a]
Lower Jurassic shale	Aerobic	0.08–0.26[b]
Yorkshire, UK	Euxinic	0.77–0.90[b]
Upper Cretaceous	Aerobic	0.09–0.79[b]
Greenhorn formation,	Dysoxic	0.67–0.87[b]
Colorado, USA		
Upper Devonian New	Aerobic	0.20–0.29[b]
Albany formation,	Dysoxic	0.46–0.78[b]
Illinois, USA	Euxinic	0.50–1.00[b]
Lower and Upper Jurrasic	Aerobic	0.17–0.43[b]
Shales UK, Germany	Dysoxic	0.48–0.71[b]
	Euxinic	0.58–0.88[b]

[a] This study.
[b] Data from Raiswell et al. (1988).

4.2. Pyrite grain morphologies

The wide variation in pyrite texture and the narrow framboid size distribution observed at Sapelo Island salt marsh suggest that caution is needed in using these criteria to determine palaeo-redox states of the environment. Previously, however, it has been proposed that

primary pyrite structures can be used as palaeoenvironmental indicators. Syngenetic pyritization (implying euxinic bottom waters) results in small size pyrite framboids, with the majority of them below 10 μm and a constant size distribution with depth (Wilkin et al., 1996). Diagenetic pyritization below dysoxic or oxic water columns results in relatively larger framboids and euhedral crystals are far more common (Suits & Wilkin, 1998). Furthermore, based on observations on ancient black shales it has been suggested that, once deposited, framboid size distribution is preserved over geologic time (Wilkin et al., 1996).

Such a depth invariant textural signature is only possible if pyritization ceases with burial and early-formed pyrite remains stable. This is the case for Black Sea sediments, which have been used as a modern example of uniform pyrite size distribution in sediments deposited in a euxinic basin (Wilkin et al., 1997, 1996). However, in the Black Sea, pyritization takes place under iron-limited conditions and iron is completely used up within the water column. No further pyritization is possible because of the lack of reactive iron in the sediment. At the Sapelo Island salt marsh, marked differences in the seasonal iron–sulfur speciation clearly indicate their rapid recycling between the aqueous and solid phase within the sediments (see Kostka et al., 2002). Such rapid changes, along with the steep chemical gradients observed in salt marsh sediments, exert a major control over pyrite morphology and its size distribution. Moreover, pyrite formation in salt marsh sediments is possible through a number of reaction mechanisms that may also influence its surface structure.

Careful analysis of pyrite grains and biogeochemical processes within the salt marsh sediment suggest that oxidative processes, SRR, reaction time and reactant availability, all control the observed resultant morphologies. At Sapelo Island, none of the pyrite framboids were of size greater than 12 μm at any depth. This may lead to the erroneous interpretation that pyritization is taking place under euxinic bottom waters. Furthermore, at the Creek Bank site, most of the pyrite was in the form of minute pyrite grains dispersed within the sediment, which may further be falsely interpreted as insufficient time for nucleation and growth or hydrodynamic instability, that is, syngenetic pyritization. At Creek Bank, despite the highest SRR and ample available reactive iron, pyrite grains do not achieve large crystal or framboid size, suggesting that pyrite is not stable. Rapid seasonal changes in pyrite concentration in the sediments further suggest that fine grained pyrite is prone to oxidation, which is controlling their size. Fused euhedral crystals and framboids are the only indications that pyrite is in fact diagenetic (Fig. 3a,b). However, it provides no indication of the extent of bottom water oxygenation because even under euxinic bottom waters such fused structures are observed if pyritization continues within the sediments (Wilkin & Barnes, 1997b).

At Ponded Marsh, on occasion, primary framboid structures, euhedral crystals and fused framboids were all observed at the same depth (Fig. 3c–e). Framboids made up of fairly uniform size microcrystal and relatively larger size framboids and euhedral crystals were observed at shallower depths (Fig. 3d,e). Framboid size decreased at depths >20 cm and fused framboids were more common. This is expected because at shallower depths, pyritization is taking place close to the O_2–H_2S interface that favors framboid formation (Wilkin & Barnes, 1996). Moreover, at shallower depths, high rates of sulfate reduction are accompanied by a larger fraction of available reactive iron that allows bathing of reactive iron in sulfide over longer periods resulting in larger grain sizes. At greater depths pyritization is limited by the availability of reactive iron and hence larger framboid sizes (>7 μm) are not attained. Although negligible SRR were observed below 10–15 cm, framboid size is not controlled by the reduction rate as downward diffusion maintains a millimolar range of dissolved sulfide in the pore waters during both seasons (Fig. 2.3c, 2.4c). Seasonal oxidation of sediments by macrophytes and bioturbation provides sufficient iron for secondary pyritization to continue at greater depths resulting in in-filled pyrite framboids. It is also possible that the oxidative processes are also responsible for reoxidizing framboids formed a priori, thereby inhibiting their growth (see Luther et al., 1982).

Puzzling though is the occurrence of concentrated pockets of loose euhedral crystals around *Spartina* roots (Fig. 3f,g). Highest SRR, as well as pyrite concentrations, were also observed around the roots. The factors contributing to the formation of euhedral crystals are not clear. In laboratory experiments, under alkaline conditions, polysulfides have been shown to produce euhedral pyrite crystals (Wilkin & Barnes, 1996). It is speculated that the *Spartina* roots are acting as conduits for oxygen transport, creating suboxic to oxic microcosms around them, and are responsible for oxidizing dissolved sulfide to zero-valent sulfur species, such as polysulfides. The high production rate of sulfide probably outcompetes oxygen diffusion thereby inhibiting complete oxidation of sulfide to sulfate.

5. Conclusions

1. In the Sapelo Island salt marsh, calculated DOP values reflect the pore water redox conditions and sediment chemistry rather than the extent of bottom water oxygenation.
2. In modern sediments, ascorbate extractable iron more accurately represents the poorly crystalline Fe mineral fraction that undergoes pyritization.

However, we concur with Raiswell et al. (1994) that over longer geologic time scales, HCl extractions are probably better for identifying the reactive iron phase.

3. Various pyrite textures observed in the sediments are the result of the complex interplay of several biogeochemical processes. Without a thorough understanding of the processes occurring at the time of pyritization, it is highly questionable to use pyrite as a palaeoenvironmental indicator of depositional environment. Furthermore, we find that the identification of pyrite textures in a statistically significant number of samples is tedious and cumbersome.
4. Caution should be applied when using DOP and pyrite grain size and texture to ascertain the extent of oxygenation within a depositional environment. This is especially true for dynamic systems where sediments are subjected to daily and seasonally oscillating environmental determinants.

Acknowledgements

This research was supported by grants from URC, University of Cape Town, South Africa, U.S. National Science Foundation (Grant No. EAR-97085350) and the U.S. Office of Naval Research (Grant No. N00014-98-1-0203). Patrick Inglette, Christof Meile and Kim Hunter are acknowledged for their expert technical help. Field support from University of Georgia Marine Institute on Sapelo Island is also acknowledged. Thanks are due to Jodie Miller for proof reading the manuscript. The authors wish to thank three anonymous journal reviewers who provided constructive criticisms and comments on the manuscript and to Dr Eric Wolanski for handling the manuscript.

References

Barnes, S. S., Craft, T. F., & Windom, H. L. (1973). Iron–scandium budget in sediments of two Georgia salt marshes. *Bulletin Georgia Academy of Science 31*, 23–30.

Basan, P. B., & Frey, R. W. (1977). Actual-palaeontology and neoichnology of salt marshes near Sapelo Island, Georgia. In T. P. Crimes, & J. C. Harper (Eds.), *Trace fossils 2* (pp. 41–70). Steel House Press.

Berner, R. A. (1970). Sedimentary pyrite formation. *American Journal of Science 268*, 1–23.

Berner, R. A. (1982). Burial of organic carbon and pyrite sulfur in modern ocean: its geochemical and environmental significance. *American Journal of Science 282*, 451–473.

Berner, R. A. (1984). Sedimentary pyrite formation: an update. *Geochimica et Cosmochimica Acta 48*, 605–615.

Berner, R. A. (1989). Biogeochemical cycles of carbon and sulfur and their effect on atmospheric oxygen over Phanerozoic time. *Palaeogeography, Palaeoclimatology, Palaeoecology 75*, 97–122.

Berner, R. A., & Landis, G. P. (1988). Gas bubbles in fossil amber as possible indicators of the major gas composition of ancient air. *Science 239*, 1406–1409.

Boesen, C., & Postma, D. (1988). Pyrite formation in anoxic environments of the Baltic. *American Journal of Science 288*, 575–603.

Buick, R. (1992). The antiquity of oxygenic photosynthesis: evidence from stromatolites in sulfate-deficient Archean lakes. *Science 255*, 74–77.

Canfield, D. E. (1989). Reactive iron in marine sediments. *Geochimica et Cosmochimica Acta 53*, 619–632.

Canfield, D. E., Raiswell, R., & Bottrell, S. H. (1992). The reactivity of sedimentary iron minerals towards sulfide. *American Journal of Science 292*, 659–683.

Canfield, D. E., Raiswell, R., Westrich, J. T., Reaves, C. M., & Berner, R. A. (1986). The use of chromium reduction in the analysis of reduced inorganic sulfur in sediments and shales. *Chemical Geology 54*, 149–155.

Cline, J. D. (1969). Spectrophotometric determination of hydrogen sulfide in natural waters. *Limnology and Oceanography 14*, 454–458.

Cutter, G. A., & Velinsky, D. J. (1988). Temporal variations of sedimentary sulfur in a Delaware salt marsh. *Marine Chemistry 23*, 311–327.

Dacey, J. W. H., & Howes, B. L. (1984). Water uptake by roots controls water table movement and sediment oxidation in short *Spartina alterniflora* marsh. *Science 224*, 487–490.

Dean, W. E., & Arthur, M. A. (1989). Iron–sulfur–carbon relationships in organic carbon rich sequences. I. Cretaceous western interior seaway. *American Journal of Science 289*, 708–743.

Fossing, H., & Jørgensen, B. B. (1989). Measurement of bacterial sulfate reduction in sediments: evaluation of a single-step chromium reduction method. *Biogeochemistry 8*(3), 205–222.

Grandstaff, D. E. (1980). Origin of uraniferous conglomerates at Elliot Lake, Canada and Witwatersrand, South Africa: implications for oxygen in the Precambrian atmosphere. *Precambrian Research 13*, 1–26.

Henderson, G. M. (2002). New oceanic proxies for paleoclimate. *Earth and Planetary Science Letters 203*, 1–13.

Hesslein, R. G. (1976). An in situ sampler for close interval pore water studies. *Limnology and Oceanography 21*, 912–914.

Howarth, R. W., & Giblin, A. E. (1983). Sulfate reduction in the salt marshes at Sapelo Island, Georgia. *Limnology and Oceanography 28*(1), 70–82.

Howes, B. L., Dacey, J. W. H., & Goehringer, D. D. (1986). Factors controlling the growth form of *Spartina alterniflora*: feedbacks between above-ground production, sediment oxidation, nitrogen and salinity. *Journal of Ecology 74*, 881–898.

Jørgensen, B. B. (1978). A comparison of methods for the quantification of bacterial sulfate reduction in coastal marine sediments. 1. Measurement with radiotracer techniques. *Geomicrobiology Journal 1*, 11–28.

Kostka, J. E., & Luther, G. W. (1994). Partitioning and speciation of solid phase iron in saltmarsh sediments. *Geochimica et Cosmochimica Acta 58*(7), 1701–1710.

Kostka, J., & Luther, G. W., III (1995). Seasonal cycling of Fe in saltmarsh sediments. *Biogeochemistry 29*, 159–181.

Kostka, J. E., Roychoudhury, A. N., & Van Cappellen, P. (2002). Rates and controls of anaerobic microbial respiration across spatial and temporal gradients in saltmarsh sediments. *Biogeochemistry 60*(1), 49–76.

Leventhal, J., & Taylor, C. (1990). Comparison of methods to determine degree of pyritisation. *Geochimica et Cosmochimica Acta 54*, 2621–2625.

Luther, G. W., III., Giblin, A. E., Howarth, R. W., & Ryans, R. A. (1982). Pyrite and oxidized iron mineral phases formed from pyrite oxidation in salt marsh and estuarine sediments. *Geochimica et Cosmochimica Acta 46*, 2671–2676.

Lyons, T. W., & Berner, R. A. (1992). Carbon–sulfur–iron systematics of the uppermost Holocene sediments of the anoxic Black Sea. *Chemical Geology 99*, 1–27.

Meile, C., Koretsky, C. M., & Van Cappellen, P. (2001). Quantifying bioirrigation in aquatic sediments: an inverse modeling approach. *Limnology and Oceanography 46*(1), 164–177.

Morse, J. W., & Wang, Q. (1997). Pyrite formation under conditions approximating those in anoxic sediments. *Marine Chemistry 57* (3–4), 187–193.

Raiswell, R., & Berner, R. A. (1985). Pyrite formation in euxinic and semi-euxinic sediments. *American Journal of Science 285*, 710–724.

Raiswell, R., Buckley, F., Berner, R. A., & Anderson, T. F. (1988). Degree of pyritization of iron as a paleoenvironmental indicator of bottom-water oxygenation. *Journal of Sedimentary Petrology 58*(5), 812–819.

Raiswell, R., & Canfield, D. E. (1998). Sources of iron for pyrite formation in marine sediments. *American Journal of Science 298*(3), 219–245.

Raiswell, R., Canfield, D. E., & Berner, R. A. (1994). A comparison of iron extraction methods for the determination of degree of pyritisation and the recognition of iron-limited pyrite formation. *Chemical Geology 111*(1–4), 101–110.

Roychoudhury, A. N. (1999). Biogeochemical dynamics in aquatic sediments; novel laboratory and field-based approaches. PhD thesis, Georgia Institute of Technology, Atlanta, GA.

Runnegar, B. (1991). Precambrian oxygen levels estimated from the biochemistry and physiology of early eukaryotes. *Palaeogeography, Palaeoclimatology, Palaeoecology 97*, 97–111.

Schidlowski, M., Appel, P. W. U., Eichmann, R., & Junge, C. E. (1979). Carbon isotope geochemistry of the 3.7×10^9-yr-old Isua sediments, West Greenland: implications for the Archean carbon and oxygen cycles. *Geochimica et Cosmochimica Acta 43*, 189–199.

Schidlowski, M., Junge, C. E., & Pietrek, H. (1977). Sulfur isotope variations in marine sulfate evaporites and the Phanerozoic oxygen budget. *Journal of Geophysical Research 82*(18), 2557–2565.

Suits, N. S., & Wilkin, R. T. (1998). Pyrite formation in the water column and sediments of a meromictic lake. *Geology (Boulder) 26*(12), 1099–1102.

Tabatabai, M. A. (1974). A rapid method for determination of sulfate in water samples. *Environmental Letters 7*(3), 237–242.

Wignall, P. B., & Newton, R. (1998). Pyrite framboid diameter as a measure of oxygen deficiency in ancient mudrocks. *American Journal of Science 298*, 537–552.

Wilkin, R. T., & Arthur, M. A. (2001). Variations in pyrite texture, sulfur isotope composition, and iron systematics in the Black Sea: evidence for late Pleistocene to Holocene excursions of the O_2–H_2S redox transition. *Geochimica et Cosmochimica Acta 65*(9), 1399–1416.

Wilkin, R. T., Arthur, M. A., & Dean, W. E. (1997). History of water-column anoxia in the Black Sea indicated by pyrite. *Earth and Planetary Science Letters 148*(3–4), 517–525.

Wilkin, R. T., & Barnes, H. L. (1996). Pyrite formation by reactions of iron monosulfides with dissolved inorganic and organic sulfur species. *Geochimica et Cosmochimica Acta 60*(21), 4167–4179.

Wilkin, R. T., & Barnes, H. L. (1997a). Formation processes of framboidal pyrite. *Geochimica et Cosmochimica Acta 61*(2), 323–339.

Wilkin, R. T., & Barnes, H. L. (1997b). Pyrite formation in an anoxic estuarine basin. *American Journal of Science 297*(6), 620–650.

Wilkin, R. T., Barnes, H. L., & Brantley, S. L. (1996). The size distribution of framboidal pyrite in modern sediments: an indicator of redox conditions. *Geochimica et Cosmochimica Acta 60*(20), 3897–3912.